Inorganic Chemistry

including bioinorganic chemistry

January 7, 2013
Volume 52, Number 1
pubs.acs.org/IC

CO_2 to Methanol Using a Nickel Catalyst

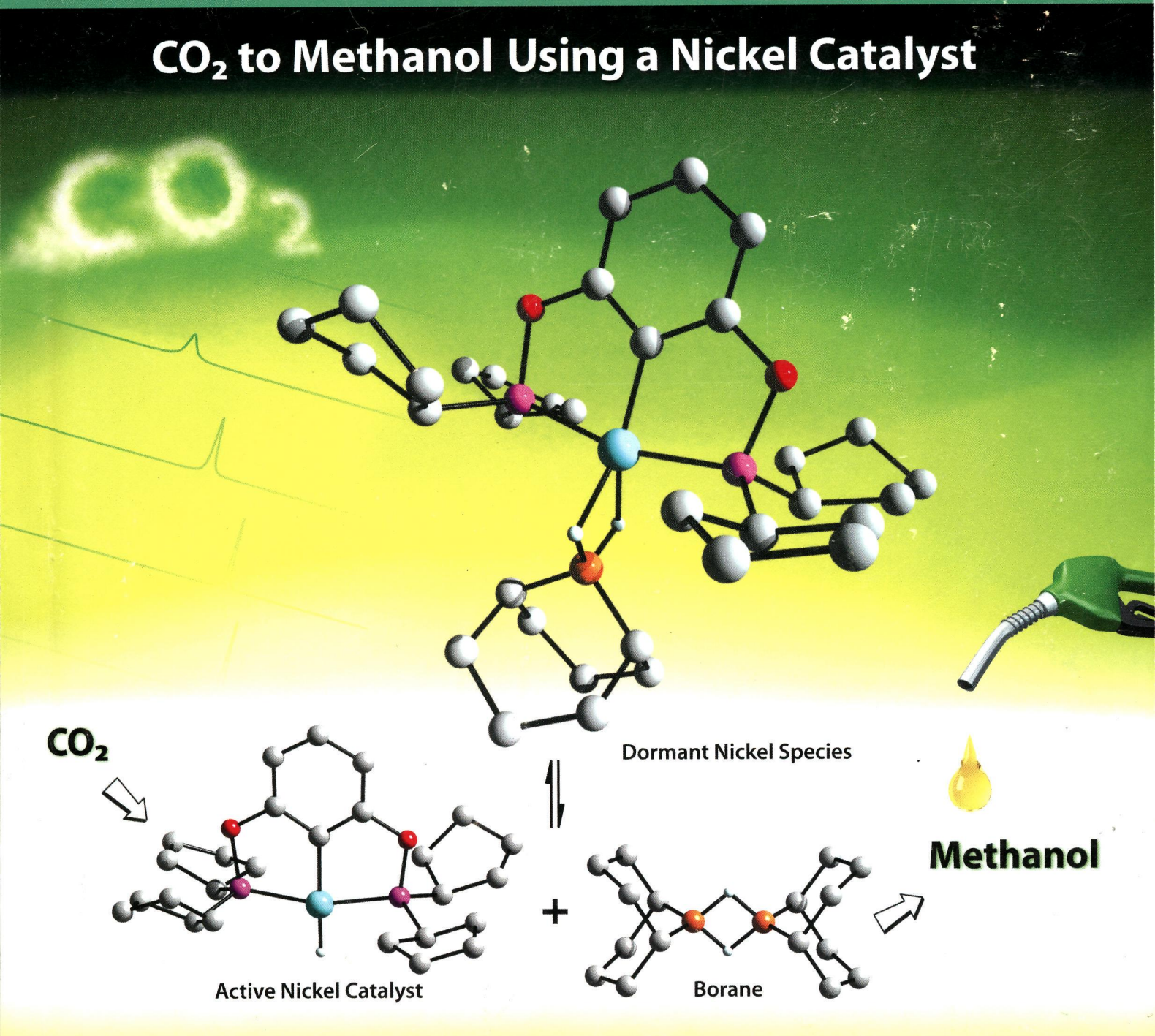

ACS Publications
MOST TRUSTED. MOST CITED. MOST READ.

www.acs.org

Inorganic Chemistry

JANUARY 7, 2013
VOLUME 52 ISSUE 1

INOCAJ 52(1) 1−528 (2013)
ISSN 0020-1669
Registered in the U.S. Patent and Trademark Office

ON THE COVER: An effective catalytic system for the hydroboration of CO_2 to methanol derivatives involves a nickel hydride complex bearing a bulky pincer ligand. Reducing the steric congestion around the hydride moiety strengthens the interaction between the nickel hydride complex and boranes, leading to the formation of catalytically dormant dihydridoborate complexes. See S. Chakraborty, J. Zhang, Y. J. Patel, J. A. Krause, and H. Guan, p 37.

Editorial

Communications

9 dx.doi.org/10.1021/ic302018g

New Facile Method for the Preparation of $M_3B_7O_{13}I$ Boracites (M = Mn, Fe, Co, Ni, Cd)

Xiu-Li Wang, Yi-Zhi Huang, and Li-Ming Wu*

Five iodine boracites, $M_3B_7O_{13}I$ (M = Mn, Fe, Co, Ni, Cd), have been synthesized by reactions of metal oxide, B_2O_3, element B, and I_2 at intermediate temperature above 350 °C. Powder X-ray diffraction analyses verify the identities and purity of the products, which are also confirmed by magnetic property measurement. Except safe, cheap, and convenient, this novel method is significantly flexible in the selection of the starting metal oxide. The influence of the reaction temperature and time has also been studied.

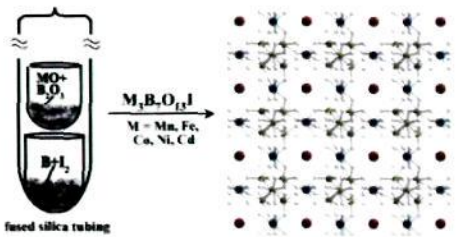

12 dx.doi.org/10.1021/ic302273h

Two-Dimensional Copper(I) Coordination Polymer Materials as Photocatalysts for the Degradation of Organic Dyes

Tian Wen, De-Xiang Zhang, and Jian Zhang*

Two isomeric two-dimensional copper(I) coordination polymer materials based on an in situ generated 5-(3-pyridyl)tetrazole ligand show similar layer structures but distinct photoluminescent and photocatalytic properties.

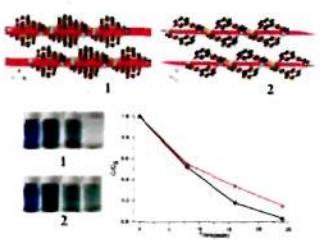

Articles

15 dx.doi.org/10.1021/ic3002509

Selectivity of the Highly Preorganized Tetradentate Ligand 2,9-Di(pyrid-2-yl)-1,10-phenanthroline for Metal Ions in Aqueous Solution, Including Lanthanide(III) Ions and the Uranyl(VI) Cation

Ashley N. Carolan, Gregory M. Cockrell, Neil J. Williams, Gang Zhang, Donald G. VanDerveer, Hee-Seung Lee, Randolph P. Thummel,* and Robert D. Hancock.*

The log K_1 values for DPP complexes of some lanthanide(III) (Ln(III)) ions in aqueous solution, as well as for alkaline-earth metal ions, and the UO_2^{2+} cation, are reported. The log K_1 values for Ln(III) ions peak at Sm(III), which is explained by MM (molecular mechanics) calculations that show that the best-fit M–N length for forming $[Ln(DPP)(H_2O)_3]^{3+}$ complexes is 2.65 Å, which also is close to the M–N length for Am(III), the target of separations from Ln(III) cations.

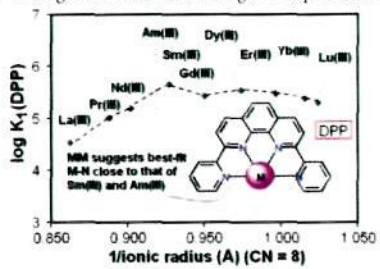

28 dx.doi.org/10.1021/ic300390s

B–H Bond Activation Using an Electrophilic Metal Complex: Insights into the Reaction Pathway

*Rahul Kumar and Balaji R. Jagirdar**

Highly electrophilic ruthenium complex $[RuCl(dppe)_2][OTf]$ brings about B–H bond activation and cleavage in ammonia borane ($H_3N{\cdot}BH_3$, AB) and dimethylamine borane ($Me_2HN{\cdot}BH_3$, DMAB). *These reactions proceed through* the intermediacy of η^1-B–H species. On the basis of detailed multinuclear variable-temperature NMR spectroscopic studies, insights into the reaction pathways of these reactions are presented.

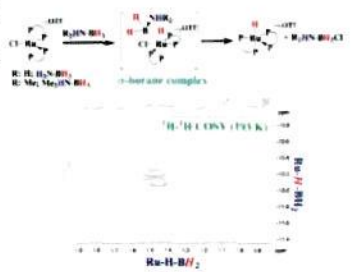

37 dx.doi.org/10.1021/ic300587b

Pincer-Ligated Nickel Hydridoborate Complexes: the Dormant Species in Catalytic Reduction of Carbon Dioxide with Boranes

Sumit Chakraborty, Jie Zhang, Yogi J. Patel, Jeanette A. Krause, and Hairong Guan*

Nickel pincer hydride complexes react with various boranes to generate nickel dihydridoborate complexes unless the pincer complexes contain bulky R groups such as *tert*-butyl groups. Depending on the boranes used, these reactions can be reversible at room temperature. In the reduction of CO_2 with boranes catalyzed by the nickel pincer hydride complexes, the nickel dihydridoborate complexes serve as dormant species outside the catalytic cycles.

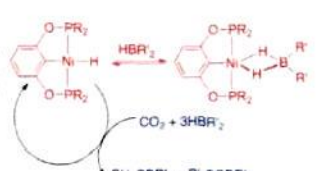

48 dx.doi.org/10.1021/ic3006508

P(CH)P Pincer Rhodium(I) Complexes: The Key Role of Electron-Poor Imidazoliophosphine Extremities

Cécile Barthes, Christine Lepetit, Yves Canac, Carine Duhayon, Davit Zargarian, and Remi Chauvin**

A bis(imidazoliophosphine) ligand-stabilized P(CH)P pincer is shown on the way to the elusive PCP adduct.

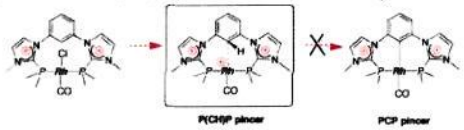

59 dx.doi.org/10.1021/ic301894e

Monomeric Bis(anilido)iron(II) Complexes with *N*-Heterocyclic Carbene Ligation: Synthesis, Characterization, and Redox Reactivity toward Aryl Halides

Xiaojie Wang, Zhenbo Mo, Jie Xiao, and Liang Deng*

The introduction of *N*-heterocyclic carbene ligand to iron amido chemistry has led to the successful preparation of a series of three- and four-coordinate mononuclear bis(anilido)iron(II) complexes. These mononuclear iron amido compounds have been fully characterized by ^{1}H NMR, solution magnetic susceptibility, UV−vis, IR, X-ray diffraction, cyclic voltammetry, as well as elemental analysis. Reactivity study showed the four coordinate dianilido complex can react with aryl iodide and bromide to afford carbon(aryl)-halogen cleavage products, but the three coordinate complex is inert toward these halides.

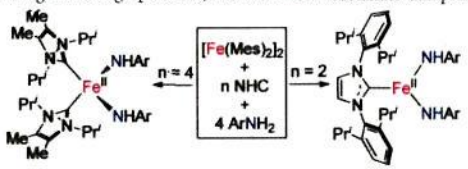

66 dx.doi.org/10.1021/ic301017g

Influence of the Substituents on the Electronic and Electrochemical Properties of a New Square-Planar Nickel-Bis(quinoxaline-6,7-dithiolate) System: Synthesis, Spectroscopy, Electrochemistry, Crystallography, and Theoretical Investigation

Ramababu Bolligarla, Samala Nagaprasad Reddy, Gummadi Durgaprasad, Vudagandla Sreenivasulu, and Samar K. Das*

The synthesis, crystal structures, spectroscopy, electrochemistry, and molecular orbital calculations of a series of square-planar nickel-bis(quinoxaline-6,7-dithiolate) complexes with the general formula $[Bu_4N]_2[Ni(X_2$6,7-qdt$)_2]$, where X = H (**1a**), Ph (**2a**), Cl (**3**), and Me (**4**) have been described. The substituents attached to the dithiolene ligands influence the electronic absorption spectra and electrochemistry of the title compounds.

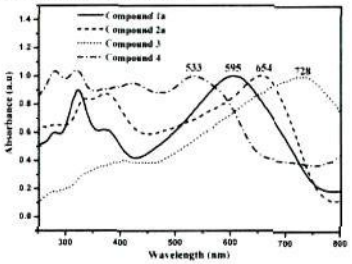

77 dx.doi.org/10.1021/ic301175f

Embedding the Ni-SOD Mimetic Ni-NCC within a Polypeptide Sequence Alters the Specificity of the Reaction Pathway

Mary E. Krause, Amanda M. Glass, Timothy A. Jackson,* and Jennifer S. Laurence*

The unique metal abstracting peptide asparagine-cysteine-cysteine (NCC) binds nickel in a square planar 2N:2S geometry and acts as a mimic of nickel superoxide dismutase. The Ni-NCC tripeptide complex undergoes rapid, site-specific chiral inversion to dld-NCC in the presence of oxygen. When the NCC sequence is embedded within longer peptides, the resulting Ni complexes do not undergo chiral inversion, but the superoxide scavenging activity of the complexes is similar to that of the chirally inverted tripeptide.

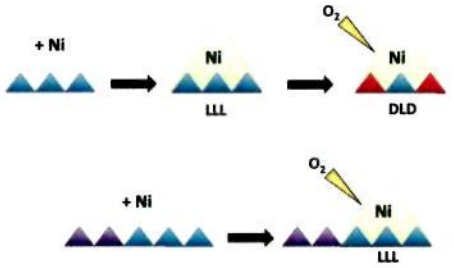

84 dx.doi.org/10.1021/ic301257k

Four New Three-Dimensional Polyoxometalate-Based Metal−Organic Frameworks Constructed From $[Mo_6O_{18}(O_3AsPh)_2]^{4-}$ Polyoxoanions and Copper(I)-Organic Fragments: Syntheses, Structures, Electrochemistry, and Photocatalysis Properties

Bo Liu, Jin Yang,* Guo-Cheng Yang, and Jian-Fang Ma*

Four novel 3D polyoxometalate-based metal−organic frameworks have been constructed from $[Mo_6O_{18}(O_3AsPh)_2]^{4-}$ polyoxoanion and different bis(triazole) ligands, and their electrochemical and photocatalytical properties have been studied in detail.

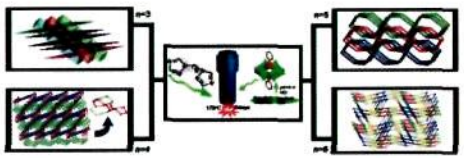

95 dx.doi.org/10.1021/ic302328e

Zinc Hydroxyacetate and Its Transformation to Nanocrystalline Zinc Oxide

Amir Moezzi, Andrew McDonagh, Annette Dowd, and Michael Cortie*

$Zn_5(OH)_8(CH_3CO_2)_2{\cdot}2H_2O$ decomposes to nanocrystalline ZnO upon calcination. The mechanism is relatively complex and involves intermediate reactions. The key feature is that 80% of the ZnO is already produced between 90 and 110 °C, while only about 20% is formed by decomposition of anhydrous zinc acetate at higher temperatures.

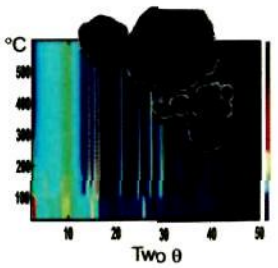

103 dx.doi.org/10.1021/ic301299e

Probing the Competition among Different Coordination Motifs in Metal–Ciprofloxacin Complexes through IRMPD Spectroscopy and DFT Calculations

Susanna Piccirillo, Alessandra Ciavardini, Enrico Bodo, Flaminia Rondino, Debora Scuderi, Vincent Steinmetz, and Alessandra Paladini*

The IRMPD spectra of ciprofloxacin complexes with monovalent (Li^+, Na^+, K^+, Ag^+) and polyvalent (Mg^{2+}, Al^{3+}) metal ions are recorded in the range 1000–1900 cm^{-1} and interpreted in the light of DFT-based quantum chemical calculations. Metal ion size and charge are found to drive the competition among different coordination motifs.

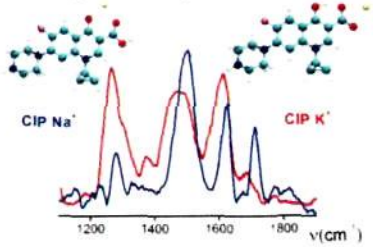

113 dx.doi.org/10.1021/ic301338a

New V^{IV}-Based Metal–Organic Framework Having Framework Flexibility and High CO_2 Adsorption Capacity

Ying-Ya Liu, Sarah Couck, Matthias Vandichel, Maciej Grzywa, Karen Leus, Shyam Biswas, Dirk Volkmer, Jorge Gascon, Freek Kapteijn, Joeri F. M. Denayer, Michel Waroquier, Veronique Van Speybroeck, and Pascal Van Der Voort*

A flexible V^{IV} based metal–organic framework VO(BPDC) featuring MIL-47 topology was synthesized. This framework shows a different profile in CO_2 and CH_4 sorption at 265 K. The in situ XRD measurements are coupled to climbing nudged elastic band calculations to find the free energy profile of the different phases.

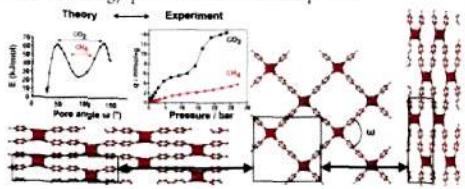

121 dx.doi.org/10.1021/ic301365y

Steady-State and Time-Resolved Investigations on Pyrene-Based Chemosensors

Javier Fernandez-Lodeiro, Cristina Núñez, Catherine S. de Castro, Emilia Bertolo, J. Sergio Seixas de Melo,* José Luis Capelo, and Carlos Lodeiro*

Colorimetric versus fluorimetric detection is shown.

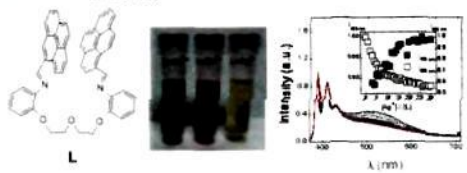

130 dx.doi.org/10.1021/ic301476p

Acid–Base Properties of the (1-4,18-36) Fragments of Neuropeptide K and their Mono- and Polynuclear Copper(II) Complexes Products of Metal-Catalyzed Oxidation

Marta Błaszak, Elżbieta Jankowska, and Teresa Kowalik-Jankowska*

Mononuclear and polynuclear complexes of (1-4,18-36)NPK and its acetylated derivative have been studied by potentiometric, UV–vis, CD, EPR spectroscopic, and mass spectrometry (MS) methods. To elucidate the products of the copper(II)-catalyzed oxidation of the (1-4,18-36)NPK and Ac-(1-4,18-36)NPK peptides the liquid chromatography–mass spectrometry (LC-MS) method and Cu(II)/hydrogen peroxide as a model oxidizing system were employed.

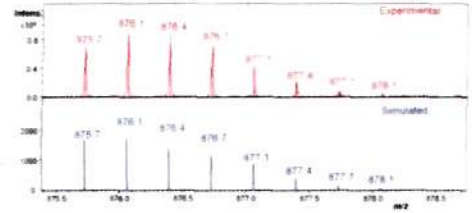

144 dx.doi.org/10.1021/ic301630d

Low-Spin Hexacoordinate Mn(III): Synthesis and Spectroscopic Investigation of Homoleptic Tris(pyrazolyl)borate and Tris(carbene)borate Complexes

Adam P. Forshaw, Jeremy M. Smith,* Andrew Ozarowski, J. Krzystek, Dmitry Smirnov, S. A. Zvyagin, T. David Harris, Hemamala I. Karunadasa, Joseph M. Zadrozny, Alexander Schnegg, Karsten Holldack, Timothy A. Jackson, Ahmad Alamiri, Diane M. Barnes, and Joshua Telser*

Three scorpionate complexes (two of bis{hydro(tris-pyrazolylborate)} and one of bis{phenyl(tris-imidazolylborate)}), $[Tp_2Mn]SbF_6$, $[Tp^*_2Mn]SbF_6$, and $[\{PhB(MeIm)_3\}_2Mn]X$ (X = CF_3SO_3, Cl), are studied. These are low-spin (S = 1) complexes of octahedral Mn(III), in contrast to the more commonly found situation for octahedral Mn(III), which is high-spin (S = 2). Field- and frequency-domain paramagnetic resonance spectroscopy techniques are used in conjunction with ligand-field theory and quantum chemical calculations (DFT, UHF) to understand the electronic structure of these complexes.

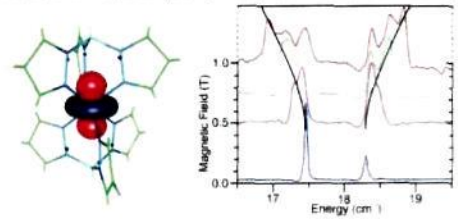

160 S dx.doi.org/10.1021/ic3015699

Phosphorescence Color Tuning of Cyclometalated Iridium Complexes by *o*-Carborane Substitution

Taewon Kim, Hyungjun Kim, Kang Mun Lee, Yoon Sup Lee,* and Min Hyung Lee*

The introduction of an *o*-carborane to the 4- and 5-position of the phenyl ring of a *ppy* ligand in heteroleptic $(C^{\wedge}N)_2Ir(acac)$ complexes gave rise to red and blue shifts of the phosphorescence band, respectively, compared to that of $(ppy)_2Ir(acac)$. PhOLED devices incorporating the 4-carborane substituted Ir(III) complex as a phosphorescent emitter displayed good performance with green phosphorescence.

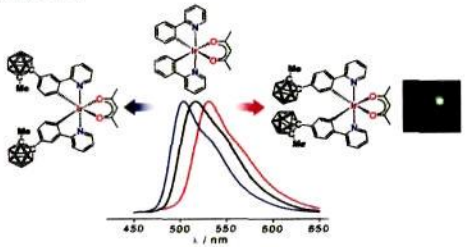

169 S dx.doi.org/10.1021/ic301573c

Proton-Induced Disproportionation of a Ruthenium Noninnocent Ligand Complex Yielding a Strong Oxidant and a Strong Reductant

Maria Kapovsky, Christopher Dares, Elaine S. Dodsworth, Rowshan Ara Begum, Vanessa Raco, and A. B. P. Lever*

The complex $Ru^{II}(NH_3)_2$(*o*-benzoquinonediimine)Cl_2 undergoes a reversible apparent acid/base reaction, although it has no obvious basic lone pairs. Disproportionation generates an oxidant ($[Ru^{III}(NH_3)_2$(*o*-benzoquinonediimine)$Cl_2]^+$) and a reductant ($[Ru^{III}(NH_3)_2$(*o*-phenylenediamine)$Cl_2]^+$). These species are characterized by UV-vis, mass, electron paramagnetic resonance (EPR), infrared (IR), and Raman spectroscopies. Their X-ray crystal data, electrochemistry, and electronic structures are detailed using density functional theory (DFT).

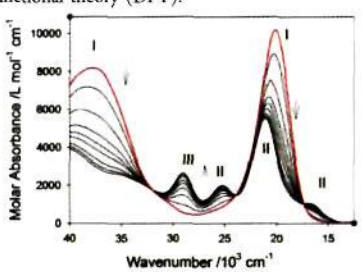

182 S dx.doi.org/10.1021/ic301577a

Preparation, Characterization, and Reactivity of Dinitrogen Molybdenum Complexes with Bis(diphenylphosphino)amine Derivative Ligands that Form a Unique 4-Membered P–N–P Chelate Ring

Takahiko Ogawa, Yuji Kajita, Yuko Wasada-Tsutsui, Hiroaki Wasada, and Hideki Masuda*

Dinitrogen molybdenum complexes bearing bis(diphenylphosphino)amine derivative ligands have been synthesized and characterized. The dinitrogen vibration value of the complexes has been affected by the dihedral angle between the P–N–P plane and N-substituent aryl group, and the P–N–P bite angle.

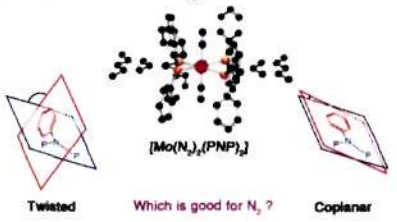

196 S dx.doi.org/10.1021/ic301592f

Density Functional Theory Studies of UO_2^{2+} and NpO_2^+ Complexes with Carbamoylmethylphosphine Oxide Ligands

Cong-Zhi Wang, Jian-Hui Lan, Yu-Liang, Zhao, Zhi-Fang Chai, Yue-Zhou Wei, and Wei-Qun Shi*

Extraction of UO_2^{2+} and NpO_2^+ from nitric acid solutions with *n*-octyl(phenyl)-*N*,*N*-diisobutylmethylcarbamoyl phosphine oxide (CMPO) was investigated.

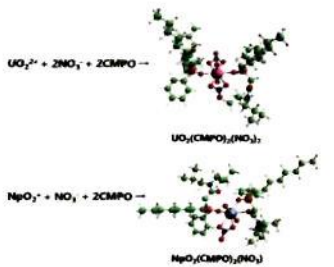

204 S dx.doi.org/10.1021/ic3016782

Systematic Analysis of the Demetalation Kinetics of Zinc Chlorophyll Derivatives Possessing Different Substituents at the 3-Position: Effects of the Electron-Withdrawing and Electron-Donating Strength of Peripheral Substituents

Yoshitaka Saga,* Yuta Kobashiri, and Kana Sadaoka

Removal of the central zinc from a series of zinc chlorophyll derivatives with a systematic variation in the electron-withdrawing and -donating substituents at the 3-position of the chlorin macrocycle was kinetically analyzed under acidic conditions. The demetalation rate constants of these derivatives possessing various electron-withdrawing and -donating groups exhibited good correlation with the Hammett σ parameters of the 3-position substituents.

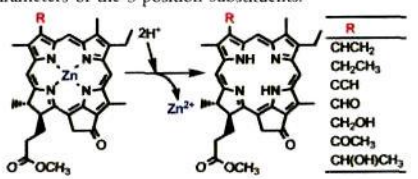

211 dx.doi.org/10.1021/ic301715n

Reactions of 11-Vertex Rhodathiaboranes with HCl: Synthesis and Reactivity of New Cl-Ligated Clusters

Beatriz Calvo, Ramon Macías,* Maria Jose Artigas, Fernando J. Lahoz, and Luis A. Oro

Reactions of 11-vertex rhodathiaboranes with HCl are presented. The clusters accommodate the acid, undergoing structural and electronic *closo*-to-*nido* transformations that demonstrate the bifunctional character of these compounds. Two new examples of stoichiometric cycles driven by Brønsted acid/base chemistry are described.

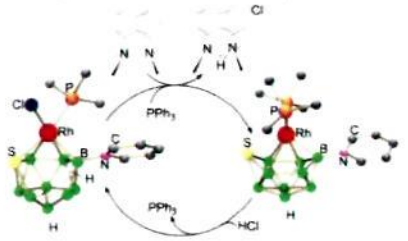

222 dx.doi.org/10.1021/ic301714d

Dinuclear Seven-Coordinate Mn(II) Complexes: Effect of Manganese(II)-Hydroxo Species on Water Exchange and Superoxide Dismutase Activity

Dominik Lieb, Felix C. Friedel, Mirza Yawer, Achim Zahl, Marat M. Khusniyarov, Frank W. Heinemann, and Ivana Ivanović-Burmazović*

We demonstrate that the dinuclear framework can offer a useful platform for increased stability of Mn(II) complexes that at the same time possess two water molecules per metal center with an increased acidity, resulting in the generation of the uniquely stable aqua-hydroxo-Mn(II) species. We examine for the first time the *trans*-effect of the hydroxide group in the case of water exchange on a divalent metal center, in general, and manganese(II), in particular.

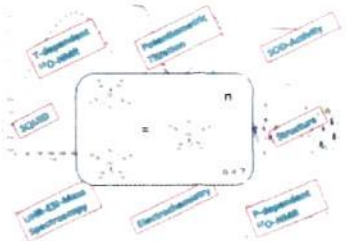

237 dx.doi.org/10.1021/ic301760a

Hydrothermal Chemistry, Structures, and Luminescence Studies of Alkali Hafnium Fluorides

Christopher C. Underwood, Colin D. McMillen, Hongyu Chen, Jeffery N. Anker, and Joseph W. Kolis*

Two ternary alkali hafnium fluorides, $LiHf_2F_9$ and $Na_3Hf_2F_{11}$, and three new alkali hafnium oxyfluorides, K_3HfOF_5, $(NH_4)_3HfOF_5$, and $K_2Hf_3OF_{12}$, have been synthesized hydrothermally and structurally characterized. X-ray and visible fluorescence studies are also discussed.

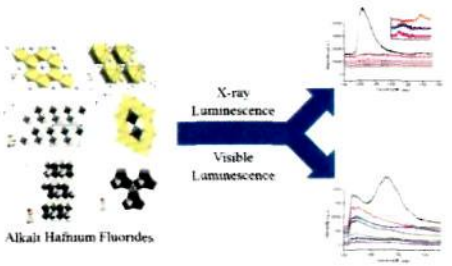

245 dx.doi.org/10.1021/ic301762g

DFT Study of Oxo-Functionalized Pentavalent Dioxouranium Complexes: Structure, Bonding, Ligand Exchange, Dimerization, and U(V)/U(IV) Reduction of OUOH and OUOSiH$_3$ Complexes

Samuel O. Odoh and Georg Schreckenbach*

The structural and electronic properties of model pentavalent oxo-functionalized dioxouranium complexes have been studied using DFT calculations. The electronic structures of these complexes are compared to those of hexavalent and pentavalent uranyl species with free oxo atoms. Several properties of these oxo-functionalized pentavalent UO_2 species such as axial−equatorial ligand exchange, dimerization, and redox potentials were explained using their electronic structures.

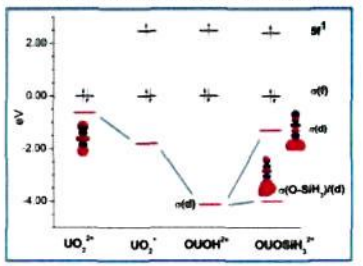

258 dx.doi.org/10.1021/ic301764t

Synthesis, Structure, and Spectroscopic and Magnetic Characterization of $[Mn_{12}O_{12}(O_2CCH_2Bu^t)_{16}(MeOH)_4]$·MeOH, a Mn_{12} Single-Molecule Magnet with True Axial Symmetry

*Christos Lampropoulos, Muralee Murugesu, Andrew G. Harter, Wolfgang Wernsdofer, Stephen Hill, Naresh S. Dalal, Arneil P. Reyes, Philip L. Kuhns, Khalil A. Abboud, and George Christou**

High symmetry plays a key role in the magnetic properties of single-molecule magnets (SMMs). The synthesis of a Mn_{12} SMM with high crystallographic symmetry and no symmetry-lowering interactions with solvent molecules of crystallization is described, along with data from extensive magnetic, high-frequency electron paramagnetic resonance, and ^{55}Mn NMR spectroscopic studies.

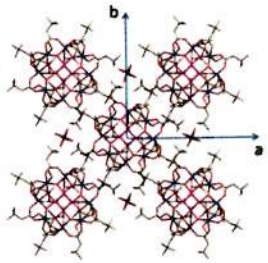

273 dx.doi.org/10.1021/ic301804n

Syntheses, Characterization, and Optical Properties of Ternary Ba–Sn–S System Compounds: Acentric $Ba_7Sn_5S_{15}$, Centric $BaSn_2S_5$, and Centric $Ba_6Sn_7S_{20}$

Zhong-Zhen Luo, Chen-Sheng Lin, Wen-Dan Cheng,* Hao Zhang, Wei-Long Zhang, and Zhang-Zhen He

Three new ternary acentric $Ba\text{-}Sn_5S_{15}$, centric $BaSn_2S_5$, and centric $Ba_6Sn\text{-}S_{20}$ were synthesized by a conventional high-temperature solid-state reaction method using the evacuated silica tubes and were characterized by X-ray diffraction and spectroscopy methods. $Ba\text{-}Sn_5S_{15}$ is a novel IR NLO crystal material with a large SHG coefficient and a wide mid-IR window. For $BaSn_2S_5$ and $Ba_6Sn\text{-}S_{20}$, they have uncommon crystal structure features in the Ba–Sn–S system.

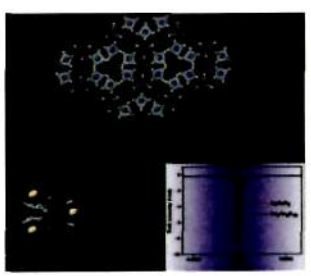

280 dx.doi.org/10.1021/ic301823j

Highly Selective CO_2 Adsorption Accompanied with Low-Energy Regeneration in a Two-Dimensional Cu(II) Porous Coordination Polymer with Inorganic Fluorinated PF_6^- Anions

Shin-ichiro Noro,* Yuh Hijikata, Munehiro Inukai, Tomohiro Fukushima, Satoshi Horike, Masakazu Higuchi, Susumu Kitagawa, Tomoyuki Akutagawa, and Takayoshi Nakamura*

High selectivity and low-energy regeneration for adsorption of CO_2 gas were achieved concurrently in a two-dimensional Cu(II) porous coordination polymer containing inorganic fluorinated PF_6^- anions that can act as moderate interaction sites for CO_2 molecules.

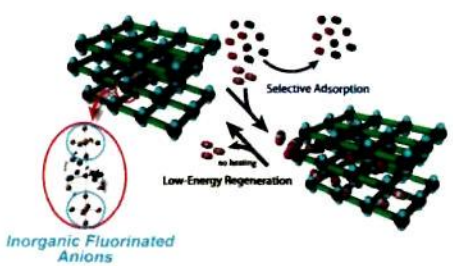

286 dx.doi.org/10.1021/ic301826s

Homoleptic Gadolinium Amidinates as Precursors for MOCVD of Oriented Gadolinium Nitride (GdN) Thin Films

Michael Krasnopolski, Cristian G. Hrib, Rüdiger W. Seidel, Manuela Winter, Hans-Werner Becker, Detlef Rogalla, Roland A. Fischer, Frank T. Edelmann,* and Anjana Devi*

Five gadolinium amidinates were synthesized and characterized in detail to evaluate them as CVD precursors. Among these compounds, the new asymmetric gadolinium amidinate $[Gd\{(NEt)(N^tBu)CMe\}_3]$ **5** showed improved thermal properties compared to the other amidinates. Compound **5** was employed to produce GdN thin films with ammonia as coreactant. For the first, we have demonstrated the formation of highly oriented GdN(200) thin films via MOCVD. The films were characterized by XRD, SEM, and RBS/NRA.

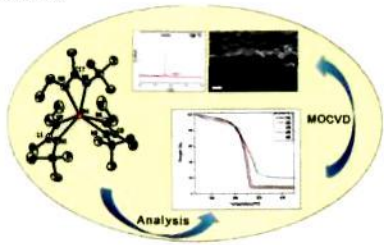

297 dx.doi.org/10.1021/ic301918x

Experimental and Theoretical Charge Densities of a Zinc-Containing Coordination Polymer, $Zn(HCOO)_2(H_2O)_2$

Mads R. V. Jørgensen, Simone Cenedese, Henrik F. Clausen, Jacob Overgaard,* Yu-Sheng Chen, Carlo Gatti, and Bo B. Iversen*

The electron density of the coordination polymer $Zn(HCOO)_2(H_2O)_2$ has been determined experimentally from X-ray diffraction data and theoretically using fully periodic density functional theory. Surprisingly, charge concentrations are found on the zinc aligned toward the negative ligands, which indicates covalency in the Zn–O bonds. These covalent contributions may be important for the magnetic interactions found in the isostructural materials containing manganese, iron, nickel, cobalt, and copper.

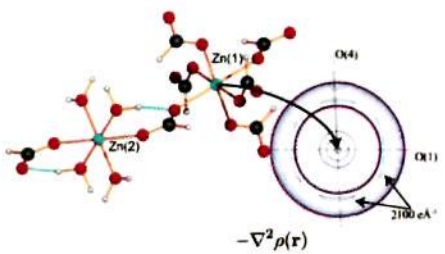

306 dx.doi.org/10.1021/ic3019277

A Donor–Acceptor Tetrathiafulvalene Ligand Complexed to Iron(II): Synthesis, Electrochemistry, and Spectroscopy of $[Fe(phen)_2(TTF\text{-}dppz)](PF_6)_2$

Nathalie Dupont, Ying-Fen Ran, Shi-Xia Liu,* Jakob Grilj, Eric Vauthey, Silvio Decurtins, and Andreas Hauser*

Light-induced population of the HS state and relaxation from an intraligand charge transfer state in an iron(II) complex with a redox-active ligand based on TTF are reported.

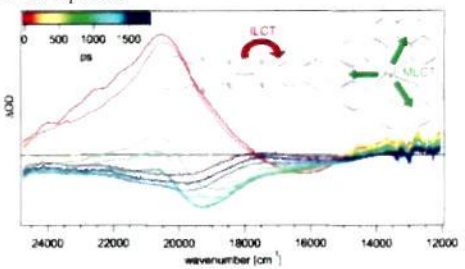

313 dx.doi.org/10.1021/ic302000j

Microwave-Assisted Synthesis, Microstructure, and Physical Properties of Rare-Earth Chromites

Jesus Prado-Gonjal, Rainer Schmidt, Juan-Jose Romero, David Avila, Ulises Amador, and Emilio Morán*

The full rare-earth (RE) chromites series (RE)CrO_3 with an orthorhombic distorted (Pnma) perovskite structure and the isostructural compound $YCrO_3$ as well can be synthesized through a simple microwave-assisted technique, yielding high-quality materials. Magnetization measurements evidence that the Néel temperature for antiferromagnetic Cr^{3+}–Cr^{3+} ordering strongly depends on the RE^{3+} ionic radius (IOR), and a rich variety of different magnetic spin interactions exists.

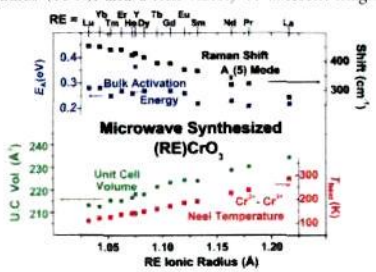

321 dx.doi.org/10.1021/ic3020755

Pyrazinoporphyrazines with Externally Appended Pyridine Rings. 13. Structure, UV–Visible Spectral Features, and Noncovalent Interaction with DNA of a Positively Charged Binuclear (Zn^{II}/Pt^{II}) Macrocycle with Multimodal Anticancer Potentialities

Ilse Manet,* Francesco Manoli, Maria Pia Donzello,* Elisa Viola, Annalisa Masi, Giuseppina Andreano, Giampaolo Ricciardi, Angela Rosa, Luciano Cellai, Claudio Ercolani, and Sandra Monti

Comparing binding to dsDNA of a water-soluble hexacationic Zn^{II} porphyrazine macrocycle containing a peripheral *cis*-platin-like functionality with that of the monometallic Zn^{II} analogue evidences a higher degree of monomerization in the presence of the Pt(II) unit in K^+-rich solution.

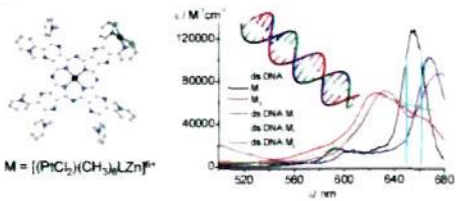

329 dx.doi.org/10.1021/ic3020805

Quintuple Bond Reactivity toward Group 16 and 17 Elements: Addition vs Insertion

Emmanuel Sobgwi Tamne, Awal Noor, Sadaf Qayyum, Tobias Bauer, and Rhett Kempe*

A dichromium complex stabilized by aminopyridinato ligands was successfully used to systematically study quintuple bond reactivity regarding group 16 and 17 elements. Insertion reactions are observed for the halogens and addition reactions for the chalcogens.

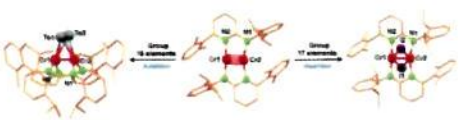

337 dx.doi.org/10.1021/ic3020817

Time-Resolved Assembly of Chiral Uranyl Peroxo Cage Clusters Containing Belts of Polyhedra

Jie Qiu, Kevin Nguyen, Laurent Jouffret, Jennifer E. S. Szymanowski, and Peter C. Burns*

Uranyl ions bridged through peroxide and phosphite ligands self-assemble into cage clusters in aqueous solution under ambient conditions. Unlike other uranyl peroxide cage clusters that are based on combinations of four-, five-, or six-membered rings of uranyl polyhedra, these are built from bands of four polyhedra, which result in unique chiral topologies.

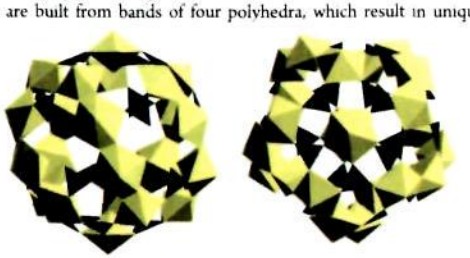

346 dx.doi.org/10.1021/ic302091t

Trimethylaluminum and Borane Complexes of Primary Amines

Balázs Németh, Jean-Paul Guégan, Tamás Veszprémi,* and Jean-Claude Guillemin*

Trimethylaluminum (TMA) complexes of primary amine derivatives were synthesized and their experimental properties and theoretical characteristics were compared with the respective amine−borane analogues. Both experimental and theoretical results support that primary amine−trimethylaluminum complexes are promising materials for MOCVD purposes.

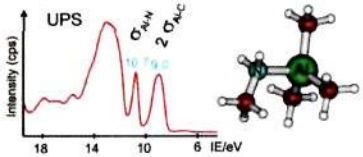

355 dx.doi.org/10.1021/ic302116b

Structural Phase Transitions on AgCuS Stromeyerite Mineral under Compression

D. Santamaria-Perez,* A. Morales-Garcia, D. Martinez-Garcia, B. Garcia-Domene, C. Mühle, and M. Jansen

The structural stability under compression of mineral Stromeyerite, AgCuS, has been studied by X-ray diffraction measurements and first-principles calculations. Two phase transitions were observed: (i) at 1.4 GPa, a first-order transition from the ambient-pressure orthorhombic $Cmc2_1$ to a tetragonal $P4/nmm$ structure, and (ii) at 5.7 GPa, a displacive second-order transition to a monoclinic $P2_1/m$ distorted phase. Cu−Cu and Ag−Ag distances comparable with those of the corresponding metallic elements were found in the high-pressure phases.

Structure of AgCuS at 3 GPa

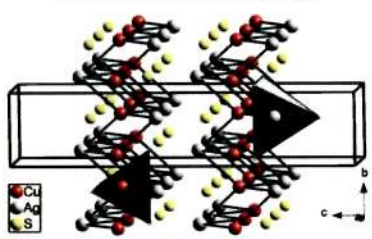

362 dx.doi.org/10.1021/ic302131n

Interaction of NO with Cu and Heme-Bound Aβ Peptides Associated with Alzheimer's Disease

Chandradeep Ghosh, Debajyoti Pramanik, Soumya Mukherjee, Abhishek Dey,* and Somdatta Ghosh Dey*

NO exposed to Cu and heme-bound Aβ peptide induces Cu oxidation coupled to heme dissociation. The electron transfer between the Cu and heme sites is mediated by the Tyr10 residue. NO, thus ameliorates the effects of reduced Cu(I) and heme binding to Aβ peptides associated with AD, providing a mechanistic pathway for its possible protective role in AD.

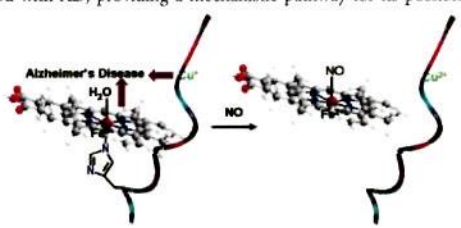

369 dx.doi.org/10.1021/ic302141z

Solvated-Ion-Pairing-Sensitive Molecular Bistability Based on Copper(I)-Coordinated Pyrimidine Ring Rotation

Michihiro Nishikawa, Kuniharu Nomoto, Shoko Kume,* and Hiroshi Nishihara*

Two rotational isomers of copper(I) complexes coexist and interconvert in solution via intramolecular ligating atom exchange of the pyrimidine ring. The values of enthalpy, entropy, and Gibbs free energy for rotation are strongly dependent on the steric demands of the diphosphine, polarity of the solvent, and size of the counterion. Consideration of solvated ion pairing is key for rationally accounting for the effect of the weak interaction on rotational equilibrium.

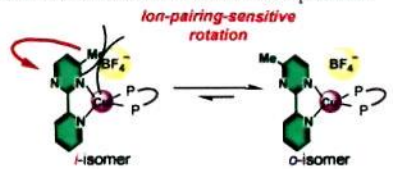

381 dx.doi.org/10.1021/ic302149p

Systematic Investigation of Relationship between Strength of NH···S Hydrogen Bond and Reactivity of Molybdoenzyme Models

Taka-aki Okamura,* Yasuhito Ushijima, Yui Omi, and Kiyotaka Onitsuka

A series of monooxomolybdenum(IV) and dioxomolybdenum(VI) complexes containing two intramolecular NH···S hydrogen bonds were synthesized and characterized by spectral and electrochemical measurements. Accurate and quantitative evaluation of NH···S hydrogen bonds revealed strong correlations among the strength of the hydrogen bond, the strength of the Mo^{VI}=O bond, and the redox potential. The hydrogen bonds stabilize the intermediate in the reaction between the monooxomolybdenum(IV) and Me_3NO, resulting in acceleration of the reaction or retardation of *trans-cis* rearrangement.

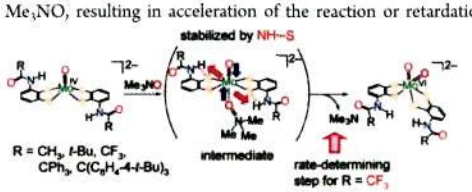

395 dx.doi.org/10.1021/ic302191d

Magnetic Structure and Properties of the $Na_2CoP_2O_7$ Pyrophosphate Cathode for Sodium-Ion Batteries: A Super-superexchange-Driven Non-Collinear Antiferromagnet

Prabeer Barpanda,* Maxim Avdeev, Chris D. Ling, Jiechen Lu, and Atsuo Yamada

The magnetic structure and properties of $Na_2CoP_2O_7$, which is a cathode material for Na^+-ion batteries, have been described by combining magnetic susceptibility, specific heat analyses, and neutron powder diffraction. It is a supersuperexchange-driven noncollinear antiferromagnet.

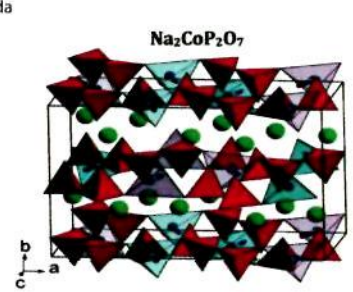

402 dx.doi.org/10.1021/ic3021996

Unprecedented Conformational Variability in Main Group Inorganic Chemistry: the Tetraazidoarsenite and -Antimonite Salts $A^+[M(N_3)_4]^-$ (A = NMe_4, PPh_4, $(Ph_3P)_2N$; M = As, Sb), Five Similar Salts, Five Different Anion Structures

Ralf Haiges,* Martin Rahm, and Karl O. Christe*

An unprecedented example for conformational variability in inorganic main group chemistry has been discovered. It is shown that small variations in the nature of the counterion and packing energies can result in five different conformers of the highly fluxional anions which have identical MN_4 skeletons but different azido ligand arrangements and very similar energies.

415 dx.doi.org/10.1021/ic3022276

Soft-Chemical Exfoliation of $RbSrNb_2O_6F$ into Homogeneously Unilamellar Oxyfluoride Nanosheets

Tadashi C. Ozawa,* Katsutoshi Fukuda, Yasuo Ebina, and Takayoshi Sasaki

A $SrNb_2O_6F^-$ nanosheet was prepared by exfoliation of layered perovskite $RbSrNb_2O_6F$. Homogeneously unilamellar nature of the exfoliated nanosheets was confirmed by X-ray scattering profile analysis and morphology observation using AFM and TEM. The optical absorption edge of the nanosheet suspension was observed around at 293 nm, and two well-defined peaks with their maxima at 229 and 278 nm were observed. Furthermore, the nanosheet suspension exhibits fluorescence emission in UV-blue region at room temperature.

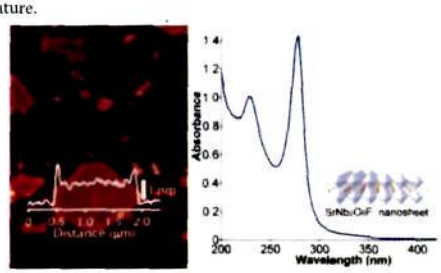

423 dx.doi.org/10.1021/ic302234j

New BDH-TTP/$[M^{III}(C_5O_5)_3]^{3-}$ (M = Fe, Ga) Isostructural Molecular Metals

Luca Pilia, Elisa Sessini, Flavia Artizzu, Masahiro Yamashita, Angela Serpe, Kazuya Kubo, Hiroshi Ito, Hisaaki Tanaka, Shin-ichi Kuroda, Jun-ichi Yamada, Paola Deplano, Carlos J. Gómez-García, and Maria Laura Mercuri*

Two new isostructural molecular metals—$(BDH\text{-}TTP)_6[M^{III}(C_5O_5)_3]\cdot CH_2Cl_2$ (BDH-TTP = 2,5-bis(1,3-dithiolan-2-ylidene)-1,3,4,6-tetrathiapentalene, where M = Fe (**1**) and Ga (**2**))—have been prepared and fully characterized. **1** is a paramagnetic molecular conductor because of the presence of isolated $[Fe(C_5O_5)_3]^{3-}$ complexes with high-spin $S = {}^5/_2$ Fe(III) metal ions. The conductivity originates from the BDH-TTP organic donors arranged in a κ-type molecular packing. It is noteworthy that, at $P >$ ~ kbar, the metal−insulator (M-I) transition is suppressed and the compound retains the metallic state down to low temperatures (2 K); in **2**, the M-I transition is not suppressed, even at pressures of 15 kbar.

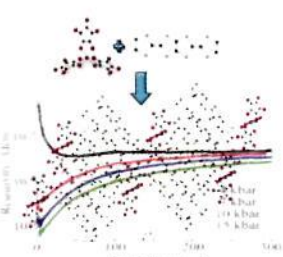

431 dx.doi.org/10.1021/ic302245x

Garnet-to-Perovskite Transition in $Gd_3Sc_2Ga_3O_{12}$ at High Pressure and High Temperature

Chuanlong Lin, Jing Liu,* Jung-Fu Lin, Xiaodong Li, Yanchun Li, Qingli Zhang, Lun Xiong, and Rui Li

Garnet-to-perovskite transition at high-pressure−temperature conditions. The inset in the upper right is the cubic garnet structure in which Gd^{3+}, Sc^{3+}, and Ga^{3+} occupy the dodecahedral, octahedral, and tetrahedral sites, respectively. The inset in the lower left is the perovskite structure in which the octahedral site is Gd^{3+} or Sc^{3+} and the dodecahedral site is Ga^{3+} or Sc^{3+}, respectively. The corresponding volumes are given.

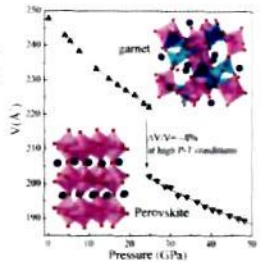

435 dx.doi.org/10.1021/ic3022744

Sulfonate Complexes of Actinide Ions: Structural Diversity in Uranyl Complexes with 2-Sulfobenzoate

Pierre Thuery*

The complexes formed by uranyl ions with the 2-sulfobenzoate dianion in the presence of different amines display a large array of structural arrangements, all containing the same seven-membered chelate ring motif. Different bridging schemes lead to zero-, one-, or two-dimensional assemblies as a result of the amine structure-directing effects and the presence of additional μ_1-oxo or μ_2-hydroxo bridges. Uranyl−3d-block metal one-dimensional heterometallic assemblies including nitrogen donors are also described.

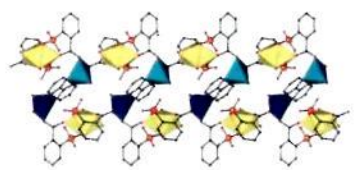

448 dx.doi.org/10.1021/ic301853t

Using Substituted Cyclometalated Quinoxaline Ligands To Finely Tune the Luminescence Properties of Iridium(III) Complexes

Emily E. Langdon-Jones, Andrew J. Hallett, Jack D. Routledge, David A. Crole, Benjamin D. Ward, James A. Platts, and Simon J. A. Pope*

Cationic, cyclometalated quinoxaline complexes of iridium(III) adorned with alkyl chains display tunable luminescent red emission in solution and solid states. The redox and electronic properties of the complexes have been comprehensively characterized using UV−vis and time-resolved luminescence spectroscopies, electrochemistry, and supporting DFT calculations.

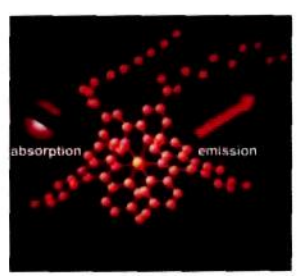

457 dx.doi.org/10.1021/ic302349f

Symmetry-Related $[Ln^{III}_6Mn^{III}_{12}]$ Clusters toward Single-Molecule Magnets and Cryogenic Magnetic Refrigerants

Jun-Liang Liu, Wei-Quan Lin, Yan-Cong Chen, Ji-Dong Leng, Fu-Sheng Guo, and Ming-Liang Tong*

Four $[Ln^{III}_6Mn^{III}_{12}]$ (Ln = Gd, Tb) nanomagnets in D_2 and C_1 molecular symmetry have been isolated. Both $[Gd^{III}_6Mn^{III}_{12}]$ possess huge but different spin ground states and significant magnetocaloric effects in a wide temperature range that maximize the refrigerant capacity, while both $[Tb^{III}_6Mn^{III}_{12}]$ behave as single-molecule magnets and exhibit symmetry-related enhancement to the effective barrier.

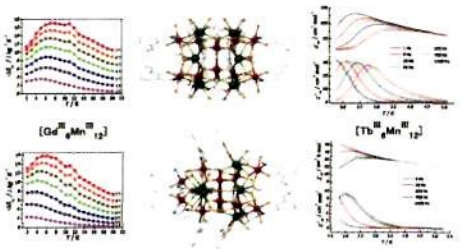

464 dx.doi.org/10.1021/ic3023437

Nitrate-to-Nitrite-to-Nitric Oxide Conversion Modulated by Nitrate-Containing $\{Fe(NO)_2\}^9$ Dinitrosyl Iron Complex (DNIC)

Fu-Te Tsai,* Yu-Ching Lee, Ming-Hsi Chiang, and Wen-Feng Liaw*

Conversion of nitrate-containing $\{Fe(NO)_2\}^9$ DNIC $[(\kappa^1\text{-}ONO_2)_2Fe(NO)_2]^-$ into N-bound nitro $\{Fe(NO)\}^6$ $[(NO)(\kappa^1\text{-}NO_2)Fe(S_2CNEt_2)_2]$ accompanied by release of N_2O_4 ($\cdot NO_2$) promoted by $(S_2CNEt_2)_2$ and then transformation of *N*-bound nitro $[(NO)(\kappa^1\text{-}NO_2)Fe(S_2CNEt_2)_2]$ into $\{Fe(NO)\}^7$ $[(NO)Fe(S_2CNEt_2)_2]$ along with release of nitric oxide and DMSO triggered by Me_2S demonstrate that nitrate-containing DNIC $[(\kappa^1\text{-}ONO_2)_2Fe(NO)_2]^-$ acts as an active center to modulate nitrate-to-nitrite-to-nitric oxide conversion.

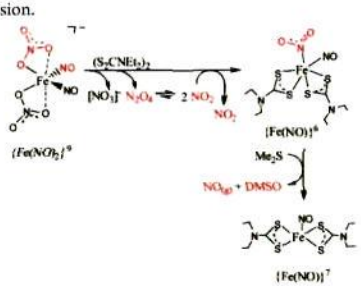

474 dx.doi.org/10.1021/ic3023584

New Insights in the Formation of Five- Versus Seven-Membered Platinacycles: A Kinetico-Mechanistic Study

Paul V. Bernhardt, Teresa Calvet, Margarita Crespo, Mercè Font-Bardía, Susanna Jansat, and Manuel Martínez*

A comprehensive kinetico-mechanistic study of the spontaneous reaction of cyclometalated platinum(IV) compounds has been conducted, and isolation of two distinct geometrical isomers producing either five or seven-membered platinum(II) cyclometalated compounds has been achieved.

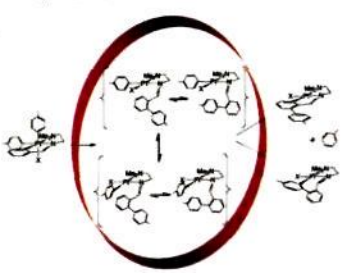

485 dx.doi.org/10.1021/ic302311q

Assembly of Organic–Inorganic Hybrid Supramolecular Materials Based on Basketlike $\{M\subset P_6Mo_{18}O_{73}\}$ (M = Ca, Sr, Ba) Cage and Transition-Metal Complex

Kai Yu, Bin Wan, Yang Yu, Lu Wang, Zhan-hua Su, Chun-mei Wang, Chun-xiao Wang, and Bai-Bin Zhou*

Four types of rigid ligands and transition metals—Cu^{2+}, Fe^{3+}, Ni^{2+}, and Cd^{2+}—have been used for construction of eight basket-based supramolecular compounds under hydrothermal conditions. The compounds display good electrocatalytic activity upon the reduction of nitrite, and fluorescent properties in the solid state at room temperature.

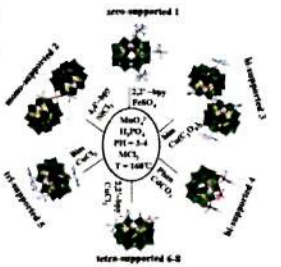

499 dx.doi.org/10.1021/ic302437t

Synthesis, Crystal and Electronic Structures of the New Zintl phases $Ba_3Al_3Pn_5$ (*Pn* = P, As) and $Ba_3Ga_3P_5$

Hua He, Chauntae Tyson, Maia Saito, and Svilen Bobev*

New Zintl compounds $Ba_3Ga_3P_5$ and $Ba_3Al_3Pn_5$ (*Pn* = P, As) have been synthesized and structurally characterized. They are isoelectronic and isotypic and crystallize with a new rhombohedral structure. The unique 3D polyanionic networks are based on corner- and edge-shared GaP_4 or $AlPn_4$ tetrahedra, forming 1D channels for the Ba^{2+} cations. The LMTO calculations on the electronic band structures suggest semiconducting behavior.

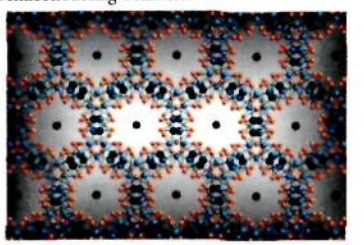

506 dx.doi.org/10.1021/ic302440g

Molecular versus Ionic Structures in Adducts of GaX_3 with Monodentate Carbon-Based Ligands

Ahmad El-Hellani, Julien Monot, Régis Guillot, Christophe Bour, and Vincent Gandon*

Adducts of GaX_3 with monodentate ligands are usually molecular species of type $L{\cdot}GaX_3$ in solution and in the solid state. We found that the reaction of some monodentate carbon-based nucleophiles of the *N*-heterocyclic carbene and 1,1-enediamine families with GaX_3 resulted in the formation of ionic compounds. A strong donor ligand tends to weaken the LGa–X bond of the X-bridged $LGaX_2(\mu\text{-}X)GaX_3$ intermediate, yielding $[L_2GaX_2][GaX_4]$.

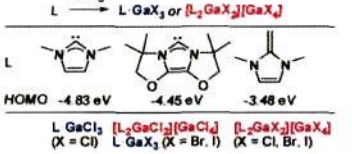

515 dx.doi.org/10.1021/ic302589b

Synthesis, Structure, and Reactivity of Iridium(III) Complexes Containing a 4,6-Dimethyl-1,3-benzenediphenylimine Pincer Ligand

Leah A. Wingard,* Mathew C. Finniss, Michael Norris, Peter S. White, Maurice Brookhart, and Joseph L. Templeton

A non-heterocyclic bis(imino)aryl ligand with blocking methyl substituents, 4,6-dimethyl-1,3- benzenediphenylimine, has been synthesized. Metallation via oxidative addition proceeds under mild conditions with $[Ir(CH_2{=}CH_2)_2(Cl)]_2$ to produce the Ir(III) product (NCN)Ir(CH_2CH_3)(Cl). Neutral nucleophiles add readily to the vacant sixth coordination site. Protonation of the ethyl group results in loss of ethane and formation of a dicationic chloride-bridged (NCN)Ir dimer. Alternatively, the chloride ligand can be abstracted from (NCN)Ir(CH_2CH_3)(Cl) to provide access to various neutral and cationic species.

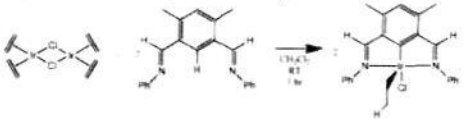

Additions and Corrections

527 dx.doi.org/10.1021/ic302621f

Correction to Preparation of a Diphosphine with Persistent Phosphinyl Radical Character in Solution: Characterization, Reactivity with O_2, S_8, Se, Te, and P_4, and Electronic Structure Calculations

Nick A. Giffin, Arthur D. Hendsbee, Tracey L. Roemmele, Michael D. Lumsden, Cory C. Pye, and Jason D. Masuda*

528 dx.doi.org/10.1021/ic302648u

Correction to Structural, Electronic, and Acid/Base Properties of $[Ru(bpy)_2(bpy(OH)_2)]^{2+}$ (bpy = 2,2′-Bipyridine, bpy(OH)$_2$ = 4,4′-Dihydroxy-2,2′-bipyridine)

Samantha Klein, William G. Dougherty, W. Scott Kassel, Timothy J. Dudley, and Jared J. Paul*

● Supporting Information available via online article